THE JOURNAL OF PHYSICAL CHEMISTRY B

ARTICLE

pubs.acs.org/JPCB

Improved DFT Description of Intrastrand Cross-Link Formation by Inclusion of London Dispersion Corrections

Céline Dupont,[†] Chandan Patel,[†] and Elise Dumont*[,†]

[†]Université de Lyon, Institut de Chimie de Lyon, CNRS, Ecole normale supérieure de Lyon, 46 allée d'Italie, 69364 Lyon Cedex 07, France

Supporting Information

ABSTRACT: The formation of covalent linkages between two vicinal nucleotides has been proved experimentally to constitute a particularly deleterious class of DNA lesions. These tandem lesions by essence present a competitive chemistry. The density functional theory with dispersion (DFT-D) method is shown to dramatically improve the theoretical description of the formation of a prototypical intrastrand cross-link, when compared to pure or hybrid GGA functionals which strongly deviate from the $\pi-\pi$ self-stacking mode, as dinucleotides are artificially stabilized by the formation of unrealistic intramolecular hydrogen bonds (HBs). Inclusion of London dispersion correction restores a more realistic picture of the reactant structure and also of geometries and energies along the reaction profile. This paves the way toward a robust in silico screening of intrastrand cross-link DNA defects.

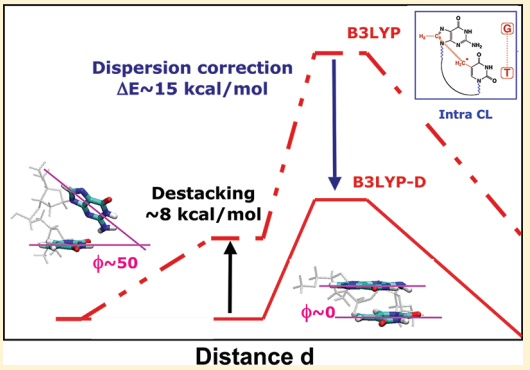

1. INTRODUCTION

DNA is continuously exposed to exogeneous and endogeneous agents that compromise its integrity.[1,2] The presence of wobble bases[3,4] and rare tautomers[5] also gives rise to DNA defects. Thus, there is an utter need to rationalize the preferential formation and outcome of DNA defects. This does not concern only the most frequent ones but also rare lesions that are associated to a lack of repair. Oxidative intrastrand cross-links (ICL) represent such an important class of chemical damage;[6] their generation in situ is triggered by reactive oxygen species.[7] These defects are formed with a lower statistic than other best-characterized lesions, such as 8-oxoguanine and thymine dimers, but they are associated with a higher mutagenicity (up to 10%[8,9]). A key difficulty in the study of tandem DNA lesions, where two nucleotides are covalently tethered, lies in the combinatorial nature of their chemistry. An example of methylene-bridged adducts is given in Figure 1; the oxidative ICLs of this family that can possibly be formed have been identified in a near exhaustive way.[10] This rather large and increasing amount of experimental data collected on tandem lesions[11] lays down some trends, but a unified understanding is hampered by nonreproducibility. The preferential formation of G8,5-MeT versus G2,5-MeT, A8, 5-MeT, A2,5-MeT, G8,5C, and so forth, and also their 3′ → 5′ strand orientation analogues, has been inferred from these experimental data. Theory is appealing to consolidate the experimentally sketched oxidative ICL selectivity. On the one side, stochastic simulations[12,13] rationalize the site of hydrogen abstraction; on the other side, energy profiles as obtained by quantum mechanics (QM) allow the identification of factors favoring some tandem lesions either from kinetic or thermodynamic perspectives:[14,15] adenine is confirmed to be less reactive,[14] while the 5′ → 3′ orientation is favored,[15] which are two electronic preferences that corroborate experimental trends. These publications exemplify how the determination of electronic activation barriers can discriminate between several possible adducts with ultimately a real predictive goal. It is to be hoped that the synergetic combination of the two approaches will overpass the individual contributions of experience or theory considered separately. To conciliate the two views, both experimental and theoretical investigations most often use dinucleotides since DNA sequence effects are known to be very limited.[9]

QM studies of DNA defect formation that have been published so far most often rely on a density functional theory framework[14,16] because of its computational practicability. Yet, most of the conventional functionals suffer from inherent deficiencies among which are self-interaction error and a lack of dispersion. Hence, geometry optimization performed with the three-parameter hybrid B3LYP functional leads to a complete loss of the ideal π-stacked structure of di- or trinucleotides.[17,18] The benefits of using recently proposed density functionals in the DNA line of research has been put forward. One can cite recent works where inclusion of dispersion[17,19−23] or use of Minnesota's M0*n* functionals[18,24] were shown to improve the structural description of di- or trinucleotides by maintaining the π-stacked mode. In this study, we have sought to evaluate the respective performance of several representative density functionals for the description of the energy profile of G8,5-MeT. We first examine pitfalls encountered with the BLYP or the equivalent B3LYP functionals.

Received: September 20, 2011
Revised: November 3, 2011
Published: November 03, 2011

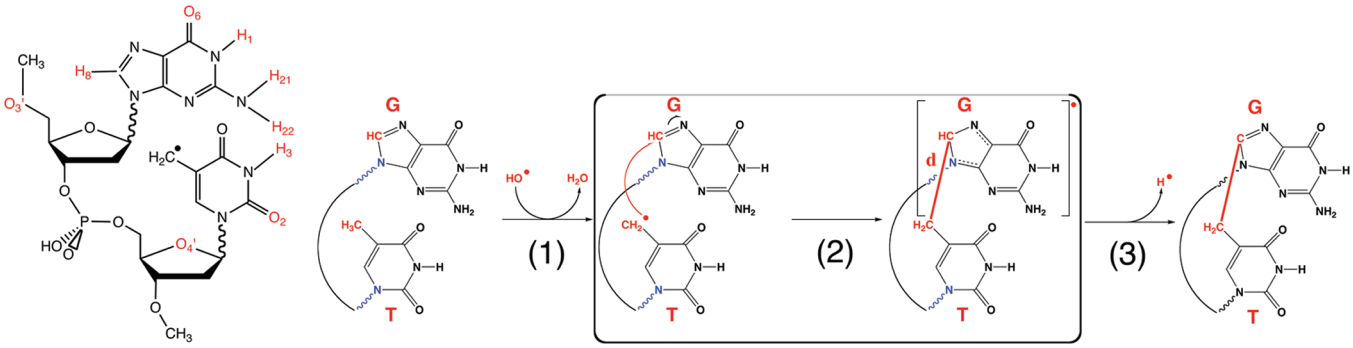

Figure 1. (left) Chemical structure of the dGpdT-H dinucleotide radical with the conventional numbering scheme. It consists of the hydrogen-abstracted pyrimidine and the radiphilic purine nucleobases, which are linked with a protonated phosphate group. (right) Three-step mechanism for the formation of the G8,5-MeT ICL adduct (radical route). Only step 2 is investigated in this study. The radical attack from H-abstracted thymine to guanine leads to a covalently tethered adduct with a bridging methylene $-CH_2-$ entity displayed with a bold red line. The *d* distance reported in red refers to the G/C8−T/C5 reaction coordinate.

Table 1. Relative Energies and Geometrical Characterization of the Three Stationary Points Characterizing the G[8,5-Me]T Formation along a Set of Representative Functionals, Dispersion-Corrected or Not (Second and First Blocks, Respectively), and Type of Hydrogen Bonds Involved in the Reactant Structure[a]

method			energetics		distance *d*			angle ϕ			HB type
family	level of theory	n^E (μ)	ΔE	$\Delta E^{\ddagger}$	R	TS	P	R	TS	P	
				Non Dispersion Corrected							
GGA	BLYP	0	8.9	22.3	6.49	2.13	1.57	55	47.9	62.6	I
H GGA	O3LYP	11.61	5.1	21.3	8.35	2.12	1.56	70.2	49.3	64.2	
	B3LYP	20	7.9	25.4	6.34	2.10	1.55	54	40.1	62.6	I
	X3LYP	21.8	7.6	25.5	6.24	2.1	1.55	53	35.7	62.4	I
	PBE0	25	3.6	23.2	6.13	2.11	1.54	52.3	34.7	65.3	I
	M06	27	0.0	14.1	4.15	2.07	1.54	15.3	32.2	56	II
H	M05	28	2.0	20.1	5.50	2.09	1.54	36.1	32.8	61.7	II
m-GGA	M06−2X	54	4.9	17.6	4.09	2.05	1.54	15.1	1.8	52.5	I
	M05−2X	56	3.7	18.8	6.24	2.04	1.54	31.8	2.4	56.6	I−II
RSH	LC-BLYP	0−100 (0.47)	3.6	27.4	5.67	2.05	1.53	46.3	2.9	55	I
	ωB97	0−100 (0.40)	4.5	23.6	5.11	2.06	1.55	34.9	2	61.1	I
	ωB97-X	15.77−100 (0.30)	−1.4	20.2	4.47	2.06	1.54	23.9	3.1	55.4	II
				Dispersion Corrected							
GGA	BLYP-D	0	6.6	13.5	5.41	2.06	1.61	43.4	0.7	5.2	I−II
	B97-D	0	2.2	9.3	3.98	2.05	1.6	20.3	2.8	7.5	
H GGA	B3LYP-D	20	−1.7	11.4	3.63	2.06	1.57	9.6	1.4	27.6	II
	ωB97-XD	22.20−100 (0.20)	−2.9	15.4	4.82	2.07	1.56	20.7	3.5	31.7	

[a] See text for more details.

The structural and energetic differences, as their dispersion-corrected versions are employed, are then discussed (section 3.2). Finally, the set of functionals is enlarged with inclusion of recently proposed functionals to assess in a more general manner the benefits of a dispersion correction.

2. COMPUTATIONAL DETAILS

All the calculations were performed with Gaussian09 program revision B.01[25] using default options and algorithms except when noted. The dGpdT motif was built up with the nucgen module of the Amber11 suite of programs[26] and was capped with methyl groups. This usual procedure prevents formation of parasitic hydrogen bonds (HBs). Sixteen density functional theory (DFT) functionals have been applied as listed per category in Table 1. Among the recently proposed functionals, we can pinpoint *meta*-GGA pure[27,28] and hybrid[29] functionals that take into account the Laplacian of the density, double hybrids[30] which explicitly are a function of the virtual orbitals, and range-separated hybrids (RSH)[31−35] in which the amount of exact exchange, n^E, depends on the interelectronic distance. In that way, contrary to the global hybrids (GH), RSH advantageously provide a physically sound description of two distant electrons. For the LC-BLYP and related functionals, the latest proposed attenuation parameter (0.47)[36] has been used. In the case of BLYP-D and B3LYP-D, a Grimme's style London dispersion correction (D2)

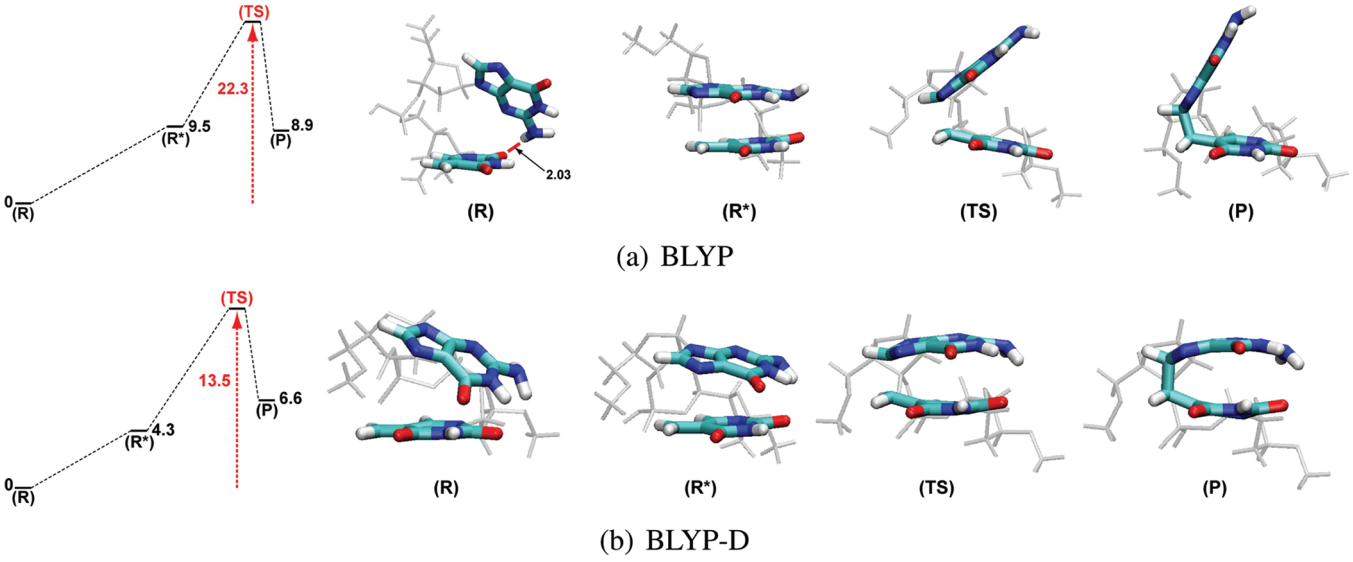

Figure 2. BLYP vs BLYP-D reaction profiles: optimized structures of reactant (**R**), constrained reactant with d = 3.6 Å (**R***), transition state (**TS**), and product (**P**). The deoxyribo−phosphate−deoxyribo *dpd* surrounding is displayed with gray lines. The red line on (**R**) represents the spurious $T/O_2-G/H_{22}$ hydrogen bond. Analogue B3LYP and B3LYP-D profiles are given in the Supporting Information.

is included;[30,37] additional tests using the dft-d3 utility[38] were performed. One verifies that the most recent D3 correction behaves very similarly to the D2 analogue. As expected, D2 contribution is slightly diminished, although differences in the two target (relative) energies are not greater than 0.5 kcal/mol.

Transition-state (TS) structures were characterized by the existence of a unique imaginary frequency corresponding to the G/C8—T/C5 mode. For the record, the $\langle S^2 \rangle$ values of the radicals never exceeded 0.77. When describing a radical reactivity, the quality of the basis set is not expected to constitute a difficulty: the double-ζ Pople basis set 6-31G(d,p) was used throughout. This hypothesis was verified by using a higher quality basis set, DZP++, including polarization and diffuse functions as described by Schaefer et al. (see, for instance, ref 39 for more details). In this case, very comparable reaction profiles are obtained with relative energies differing by less than 1 kcal.mol^{-1} (see the Supporting Information).

3. RESULTS AND DISCUSSION

The distance $d \equiv$ d(G/C8−T/Me-C5) between the thymine-methyl carbon (C5) and a given center of the purine bases (here C8, the most prone to stabilize an unpaired spin density[40]) constitutes the most natural one-dimensional reaction coordinate to describe the cyclization. The second step (2) (Figure 1) is the sole one where the two nucleobases are simultaneously implicated. We begin the analysis by commenting on the G8,5-MeT profile as computed with the two functionals BLYP and B3LYP. The first one is chosen as the most commonly used notably in first-principle molecular dynamics (MD) simulations,[40] while its three-parameter hybrid analogue is a most popular functional when describing molecular reactivity and DNA more specifically.[14,15,41] We then demonstrate how inclusion of dispersion strongly alleviates the discrepancies in maintaining the self π-stacked structure reactant and, hence, energy overestimation. The behavior of other functionals, dispersion-corrected or not, is then investigated in a more general way.

3.1. BLYP and B3LYP Profiles: Pathology of Nondispersion-Corrected Approaches. The second step of G8,5-MeT formation is investigated using the pure GGA functional BLYP and the three-parameter hybrid B3LYP density funtionals. A first result is that both functionals present very similar behaviors, and hence, only BLYP results are discussed here, while those for B3LYP are reported in the Information. Cartoon representations of optimized structures for the three stationary points, namely, reactant (**R**), transition state (**TS**), and product (**P**), and their energies are reported in Figure 2 as well as the enforced structure (**R***) with d = 3.6 Å. We start the analysis of this reaction profile by commenting on the reactant structure. It deviates notably from the π−π self-stacking mode as captured by monitoring the guanine−thymine plane-to-plane dihedral angle ϕ. From its initial zero value, it reaches 55° for (**R**) after geometry optimization. This angular opening corresponds to a flip of the guanine with respect to the thymine. This destacking is driven by the formation of a stabilizing intramolecular HB between one hydrogen of the guanine amino group and an available oxygen, here from a ketonic function of the thymine nucleobase, at a distance $d(T/O_2...G/H_{22}-N)$ of 2.03 Å following the numerotation adopted in Figure 1, leftside. Consequently, d increases up to 6.5 Å, which is an approaching distance that is with little doubt overestimated. Labet et al. came to the same conclusion when obtaining a value of 7.32 Å using the B3LYP functional.[15,42]

This geometrical inspection of BLYP (or equivalently B3LYP) optimized guanine−thymine dinucleotides surmises a pitfall of these functionals to correctly maintain the π-stacked mode, the most representative 0 K structure of a dinucleotide.[21] The conformational landscape spanned by an isolated dinucleotide is significantly more complicated and hence more difficult to sample than the same motif embedded within a dodecamer.[43] Yet, within a static, electronic-only description, one considers the lowest-energy structure as the most representative one with no exploration of the potential energy surface. An interesting intermediate structure is the enforced structure (**R***) with a distance d taken as 3.6 Å, that is, its value in a B-helix structure.

The energetic cost for passing from the fully optimized reactant ((**R**), d = 6.5 Å) to (**R***) is quantified to 9.5 kcal.mol^{-1} with the BLYP functional (8.2 with the B3LYP functional); this increment partly accounts for the disruption of so-formed intramolecular HBs. It contributes significantly (ca. 40%) to the activation barrier toward formation of the methylene-bridged ICL, G8,5-MeT. A lower value of the total activation energy would lie in better agreement with the experimentally established feasibility of the damage process and also with values usually computed for other radical processes in biochemistry typically ∼10−15 kcal.mol^{-1}.[40,44]

Besides, the structural pitfall of BLYP functional does not only affect the reactant but is experienced along the whole reaction path. The transition state ((**TS**), $d^{\ddagger} \sim 2.1$ Å) and the structurally close product (**P**) also suffer from a lack of π-stacking because of the absence of London dispersion forces in (hybrid) GGA functionals. They are significatively bent (48 and 63°). These optimized values of ϕ result from a compromise between formation of the intramolecular HBs, which are no longer observed after $d \approx 2.4$ Å, and the formation of the carbon−carbon covalent T(Me-C5)/G(C8) linkage that locks the conformation.[40] The overbend of product prevents a sound prediction of endothermicities, hence the use of a thermodynamic argument for the relative stabilities of a collection of DNA defects.[45] At this stage, it is legitimate to circumvent this destacking by imposing an additional geometrical constraint in order to improve the gas-phase description of G8,5-MeT formation; such a choice has been done in the seminal time-dependent density functional theory description of thymine dimer 2 + 2 cycloaddition by Durbeej and Eriksson.[16] This analysis urges us to provide a more faithful geometrical description of the different structures along the reaction profile. As the lack of π-stacking is clearly responsible for the deficiencies in the reaction profile, we shall consider the inclusion of an explicit R^{-6} dependence, as formulated by Grimme (D2[30,37]), on the original BLYP functional and on the hybrid B3LYP functional as a possible physically sounded solution to palliate its pitfall.

3.2. Impact of a Dispersion Correction: BLYP-D and B3LYP-D Profiles. The dispersion-corrected BLYP-D reaction profile is given in Figure 2b along with cartoon representations of the optimized stationary points. Optimization of the isolated reactant dGpdT-H is strongly impacted by inclusion of the dispersion-correction. (**R**) appears visually to be more planar as confirmed by a slightly decreased ϕ angle (43°). The structural inspection also reveals that guanine now approximately stacks right over the thymine in sharp contrast to the BLYP structure where the two nucleobases were shifted. As a result, the approaching distance d is decreased by ca. 1 Å. Accordingly, the T/O_2...G/H_{22}−N hydrogen bond is significantly lengthened, while another HB between G/H_{21} and an available oxygen from the deoxyribo ring of thymine, namely, O_4' comes into play (both at a distance of ∼2.3 Å). This rather shy, nascent structural difference becomes more clear between the B3LYP and B3LYP-D functionals (see the Supporting Information).

Employing BLYP-D nevertheless has a direct impact on activation energy: $\Delta E^{\ddagger}$ drops from 22.3 to 13.5 kcal.mol^{-1}. This decrease can be traced back to (1) the energetic reducing between (**R**) and (**R***) from 9.5 to 4.3 kcal.mol^{-1} and (2) an additional stabilization of the TS structure with respect to the reactant as (**TS**) recovers a near-exact planarity (ϕ of 0.7 vs 47.9°). This results in an earlier TS with a shorter critical distance $d^{\ddagger}$ of 2.06 Å. Here, the dispersion correction is not only experienced by the reactant (**R**) but influences the whole reaction path. The cross-linked adduct (**P**) also exhibits a remarkable structural difference with a guanine/thymine plane-to-plane angle ϕ as low as 5° inducing a less constrained C−C bond for which a distance of 1.61 Å is computed. Endothermicity for the cyclization process $\Delta E_{R\rightarrow P}$ is lessened from 8.9 in absence of D-correction to 6.6 kcal.mol^{-1}. The $\Delta E_{R\rightarrow R^*}$ increment is significantly diminished (and even canceled for B3LYP-D).

The inspection of the four profiles for the G8,5-MeT ICL formation shows how the inclusion of an empirical dispersion correction dramatically improves the DFT description of a DNA tandem lesion formation. These calculations surmise the importance of London forces in avoiding a marked deviation from the most representative self-stacked structure independently of the choice of a D2 versus D3 formalism.

3.3. A More General Assessment of Density Functional Theory with Dispersion (DFT-D) Performance. Reaction profiles have been determined using 12 functionals beyond the BLYP/B3LYP and BLYP-D/B3LYP-D cases. For sake of conciseness, we have collected in Table 1 the two key energetic quantities $\Delta E^{\ddagger}$ and $\Delta E_{R\rightarrow P}$ as well as a set of structurally determining parameters (d and ϕ) for the three stationary points (**R**), (**TS**), and (**P**). Existing intramolecular hydrogen bonds within the reactant optimized structure are detailed in the Supporting Information.

In the first section of Table 1, non-dispersion-corrected functionals are classified into three categories: pure and hybrid GGAs, *meta*-GGA hybrids, and range-separated hybrids (RSHs). The percentage of exact exchange (n^E) ranges from 11.6 and 56%, which covers the largest values usually employed.[46] A comparison of most popular functionals such as B3LYP or the fitted-free PBE0 performance against recently proposed ones, such as Minnesota's M0n(2X) functionals and range-separated hybrids—either LC-BLYP (Hirao's scheme) or Head-Gordon's ωB97(X)—is discussed throughout.

We shall first consider the four hybrid GGA functionals. This loss of π-stacking is exemplified by the B3LYP optimized reactant (**R**) represented in Figure 3 (bottom left). Its structure features a spurious nucleobase—nucleobase T/$O_2\cdots$G/H_{22} intramolecular HB even slightly shorter than predicted with the BLYP functional (d_{HB} = 2.00 vs 2.03 Å). In the analysis in section 3.1, the price to pay for the formation of the (artificial) stabilization is an angular opening, which ultimately leads to an overestimation of $\Delta E^{\ddagger}$ as one describes the G∧T cyclization. The same observation stands for the four hybrid GGA functionals (data in Table 1). Increasing the amount of exact exchange n^E to ∼20−25% does not improve over the BLYP pitfall (when comparing to the set of functionals from O3LYP to X3LYP). The four hybrid GGA functionals predict $\phi_{(R)}$ angles greater than 52° (up to 70° for the O3LYP functional). Consequently, the starting approaching distance d overpasses 6.1 Å, which is considerably higher than the B-DNA like 3.6 Å value. It can be noted that ϕ and d approximately obey a linear dependence; see the Supporting Information. The latter is barely functional-dependent but rather reflects a dinucleotide structural property. Upon (hybrid) GGA-DFT optimization, deviation of (**R**) from the π self-stacked mode uniformly leads to high activation energy barriers greater than 21 kcal.mol^{-1}.

The behavior of other non-dispersion-corrected functionals, either *meta*-GGA or RSH ones (remaining blue and red bars in Figure 3), is now discussed. On the basis of previous post Hartree−Fock investigations,[18] one can retain an upper bound for the reactant GT angle $\phi_{(R)}$ of 20°. This geometrical criterion, represented with a dashed line on the ordinate of Figure 3, is not verified by any hybrid GGA functionals and also rules out most *meta*-GGA functionals.

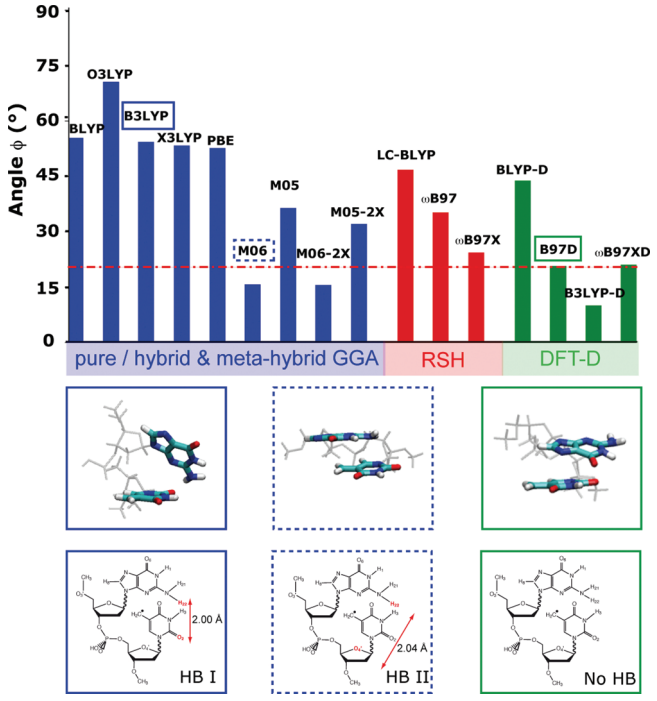

Figure 3. $\phi_{(R)}$ values along the set of density functionals, either pure or hybrid (meta)GGA; range-separated hybrids (RSH); and four dispersion-corrected functionals. The red alternate dashed line denotes an upper bound of 20° for the ϕ angle. Cartoon representations for three representative functionals are given to illustrate type **I** vs **II** hydrogen bonds with involved atoms reported in red.

While the poor behavior of hybrid GGAs clearly stands out, the *meta*-GGA M06 functional significantly improves over the structural description of (**R**) $\phi \sim 15°$ again independently of the amount of exact exchange (twice in the 2X version). As a result, $d_{(R)}$ is decreased from ca. 6.2 to 4.1 Å, and activation energies lie in the range of 14—18 kcal.mol^{-1}. One verifies that, as expected, an increase of n^E often leads to an increase of $\Delta E^{\ddagger}$ with the exception of M05 versus M05−2X. A closer inspection of HB pairing (as inventoried in the Supporting Information) reveals that the interaction between one hydrogen of the guanine amino group and oxygen of thymine is no longer formed. Instead, the same kind of intramolecular HB as obtained with BLYP-D between guanine amino hydrogens and the lateral chain is observed; it is weaker with a distance $T/O_4' \cdots G/H_{22}$ comprised between 2.1 and 2.4 Å. These two HBs clearly play different roles on the reactant geometry. Intramolecular comparison of the optimized reactant structures obtained at the B3LYP and M06 levels (cartoon representations of Figure 3) reveals that the first type of HB (between nucleobases) induces an opening of the structure by linking the two bases, whereas the second HB (between guanine ring and thymine deoxyribo) involves a near alignment of the guanine ring with the deoxyribo thymine chain hence leading to a more packed structure. Contrary to the two functionals, M06 and M06−2X, M05 and M05−2X were not found to benefit from such an improvement. All structures featuring a type I HB are associated with a large activation energy barrier (17.6 kcal.mol^{-1} and higher), whereas the presence of a type II HB tends to correspond to low activation energy barriers inferior to 14.1 kcal.mol^{-1} as listed in Table 1.

Finally, we can briefly comment on the mitigated performance of RSH functionals (LC-BLYP, ωB97, and ωB97X). Geometrical criteria are slightly improved: $\phi_{(R)}$ ranges between 24 and 46°, and *d* ranges between 4.5 and 5.7 Å; see Figure 3. One strong intramolecular HB, of one of the two classes, is present in each structure. RSH functionals give a wrong description of this radical process with activation barriers still larger than 20 kcal. mol^{-1} in sharp contrast to the M06(−2X) functionals. Yet, even for these two functionals, the final product structure is significantly bent. Nevertheless, the large ϕ angles (56°) obtained for the products suggest that London forces are not yet correctly accounted for.

In conclusion, none of the functionals neglecting the dispersion contribution leads to a satisfactory description of the reaction path either energetically or geometrically speaking. In all these cases, the origin of the spurious deviation is the formation of artificial intramolecular HBs allowed by the absence of π-stacking. This analysis urges us to consider in a systematic way the inclusion of dispersion in line with the BLYP versus BLYP-D contrasted situation.

DFT-D results are collected in the second section of Table 1. The difference with the uncorrected functionals is striking. Three out of four dispersion-corrected functionals satisfy the planarity condition we imposed on $\phi_{(R)}$ as can be seen on the third cartoon representations in Figure 3 given for the B97-D functional. It is remarkable that one restores a more satisfactory reaction profile whatever the level of sophistication of the DFT-D functional. The improvement induced by dispersion does not depend on the model used for the correction. In fact, both Grimme's (BLYP-D, B3LYP-D, and B97-D) and Head-Gordon's (ωB97X-D) formalisms for taking into account London forces lead to better reaction profiles. Hence, the stacked mode is nicely maintained along the whole reaction path: $\phi_{(P)}$ does not overpass 32°. Following the approximate linear cross-dependence between ϕ and *d*, the approaching distance in the reactant is also reduced as soon as DFT-D functionals are employed. $d_{(R)}$ is equal to 3.98 and 3.63 Å, respectively for BLYP-D and B3LYP-D, and this better geometrical description comes along with a marked decrease of activation energies. They are roughly divided by two within a DFT-D framework. $\Delta E^{\ddagger}$ ranges between 15.4 and 9.3 kcal.mol^{-1}, respectively, for the RSH ωB97XD functionals and the pure GGA Grimme's B97-D. Finally, we have to mention that the possibility of single-point calculations on geometries obtained with another density functional was not considered here; however, it is interesting, for instance, that the M06−2X/B97-D combo has proved to be efficient for computational studies of spontaneous mutation.[47] This indicates, satisfactorily enough, that these recently proposed functionals improve in a more general manner the theoretical description of DNA reactivity.

At this stage, one lacks here a high-level reference post Hartree−Fock calculation to benchmark the best functional in terms of accuracy. Nevertheless, one cannot here seek an absolute calibration all the more since the second-order Möller-Plesset MP2 method would not suffice and one would need a CCSD(T) reference calculation. We do not conclude on the more suited functionals between ωB97-XD and B3LYP-D for instance. The main conclusion is that any dispersion-corrected functionals will lead in turn to the same predictions concerning the relative formation of some intrastrand cross-link adducts.

4. CONCLUDING REMARKS

In the DNA tandem lesion line of research, it is desirable to benefit from a modeling approach capable of ensuring a reliable

description (or even prediction) of their structure and ease of formation. A key issue lies in the combinatorial nature of oxidative ICL formation. As first-principle simulations are too computationally demanding to be used for screening purposes to deal with a combinatorial chemisty, alternative strategies have to be tailored. Within the framework of our study, it appears that almost all of the hybrid density functionals provide similar reaction pathways in terms of energy; notably, optimized structures strongly deviate from the stacked mode.

In this study, it is demonstrated that it is critical to have a faithful estimate of the planar, most representative dinucleotide structure; otherwise, d and in turn $\Delta E^{\ddagger}$ are impacted upon formation of spurious intramolecular hydrogen bonds. DFT-D affords a spectacular improvement in preserving the most representative, stacked structure. It can be promoted as a useful computational tool to screen several possible conformers for oxidative tandem ICLs such as methylene-bridged lesions of the G8,5-MeT family and also newly elucidated intrastrand cross-links either oxidative[48] or light-induced[49] for which no selectivity rules have yet been inferred.

■ ASSOCIATED CONTENT

Supporting Information. Energy profiles and cartoon representations of the three stationary points for B3LYP versus B3LYP-D profiles. ($d_{(R)}$, $\phi_{(R)}$) plot for the values of Table 1. Auxiliary calculations concerning the basis set dependence. Inventory of the HB distances in the optimized reactant structures (Table 2). This material is available free of charge via the Internet at http://pubs.acs.org/.

■ AUTHOR INFORMATION

Corresponding Author
*E-mail: elise.dumont@ens-lyon.fr.

■ ACKNOWLEDGMENT

Ab initio calculations were performed using the local HPC resources of PSMN at ENS-Lyon and of GENCI (CINES/IDRIS) project x2011075105. We sincerely acknowledge Prof. André Grand, Vanessa Labet, and Christophe Morell for scientific discussions. We are grateful to Paul Fleurat-Lessard for his helpful comments on the manuscript.

■ REFERENCES

(1) Bont, R. D.; van Larebeke, N. *Mutagenesis* **2004**, *19*, 169–185.
(2) Scharer, O. D. *ChemBioChem* **2005**, *6*, 27–32.
(3) Sponer, J.; Jurecka, P.; Hobza, P. *J. Am. Chem. Soc.* **2004**, *126*, 10142–10151.
(4) Brown, K. L.; Basu., A. K.; Stone, M. P. *Biochemistry* **2009**, *48*, 9722–9733.
(5) Wang, W.; Hellinga, H. W.; Beese, L. S. *Proc. Natl. Acad. Sci.* **2011**, *108*, 17644–17648.
(6) Kanvah, S.; Joseph, J.; Schuster, G. B.; Barnett, R. N.; Ceveland, C. L.; Landman, U. *Acc. Chem. Res.* **2010**, *43*, 280–287.
(7) Wiseman, H.; Halliwell, B. *Biochem. J.* **1996**, *313*, 17–29.
(8) Yang, Z.; Collis, L. C.; Basu, A. K.; Zou, Y. *Chem. Res. Toxicol.* **2006**, *18*, 1339–1346.
(9) Gu, C.; Zhang, Q.; Yang, Z.; Wang, Y.; Zhou, Y.; Wang, Y. *Biochemistry* **2006**, *45*, 10739–10746.
(10) Their structural elucidation and screening rely on tandem mass spectrometry coupled to high-performance liquid chromatography, the sole technique with a detection threshold as low as 1:10^9.
(11) Gates, K. S. *Rev. React. Intermed. Chem.* **2007**, *8*, 333–378.
(12) Balasubramanian, B.; Pogozelski, W. K.; Tullius, T. D. *Proc. Natl. Acad. Sc.* **1998**, *343*, 9738–9743.
(13) Begusova, M.; Spotheim-Maurizot, M.; Sy, D.; Michalik, V.; Charlier, M. *J. Biomol. Struct. Dyn.* **2001**, *19*, 141.
(14) Xerri, B.; Morell, C.; Grand, A.; Cadet, J.; Cimino, P.; Barone, V. *Org. Biomol. Chem.* **2006**, *4*, 3986–3992.
(15) Labet, V.; Morell, C.; Grand, A.; Cadet, J.; Cimino, P.; Barone, V. *Org. Biomol. Chem.* **2008**, *6*, 3300–3305.
(16) Durbeej, B.; Eriksson, L. A. *Photochem. Photobiol.* **2003**, *78*, 159–167.
(17) Guerra, C. F.; van der Wijst, T.; Poater, J.; Swart, M.; Bickelhaupt, F. M. *Theor. Chem. Acc.* **2010**, *125*, 245.
(18) Gu, J.; Wang, J.; Leszczynski, J. *Chem. Phys. Lett.* **2011**, *512*, 108–112.
(19) Morgado, C.; Vincent, M. A.; Hillier, I. H.; Shan, X. *Phys. Chem. Chem. Phys.* **2007**, *9*, 448–451.
(20) Poater, J.; Swart, M.; Guerra, C. F.; Bickelhaupt, F. M. *Chem. Commun.* **2011**, *47*, 7326–7328.
(21) Lin, I.-C.; Rothlisberger, U. *Phys. Chem. Chem. Phys.* **2008**, *10*, 2730–2734.
(22) Burns, L. A.; Vazquez-Mayagoitia, A.; Sumpter, B. G.; Sherrill, D. C. *J. Chem. Phys.* **2011**, *134*, 084107.
(23) Thanthiriwatte, K. S.; Hohenstein, E. G.; Burns, L. A.; Sherrill, D. C. *J. Chem. Theory Comput.* **2011**, *7*, 88–96.
(24) Hohenstein, E. G.; Chill, S. T.; Sherrill, D. C. *J. Chem. Theory Comput.* **2008**, *4*, 1996–2000.
(25) Frisch, M. J.; et al. *Gaussian 09*, revision B.01; Gaussian Inc.: Wallingford, CT, 2009.
(26) Case, D.; et al. *AMBER 11*; University of California: San Francisco, CA, 2010.
(27) Van Voorhis, T.; Scuseria, G. E. *J. Chem. Phys.* **1998**, *109*, 400–410.
(28) Becke, A. D. *J. Chem. Phys.* **1996**, *104*, 1040–1046.
(29) Zhao, Y.; Truhlar, D. G. *Acc. Chem. Res.* **2008**, *41*, 157–167.
(30) Grimme, S. *J. Chem. Phys.* **2006**, *124*, 034108.
(31) Savin, A. In *Recent Developments and Applications of Modern Density Functional Theory*; Seminario, J. M., Ed.; Elsevier: Amsterdam, 1996; Chapter 9, pp 327−354.
(32) Iikura, H.; Tsuneda, T.; Yanai, T.; Hirao, K. *J. Chem. Phys.* **2001**, *115*, 3540–3544.
(33) Yanai, T.; Tew, D. P.; Handy, N. C. *Chem. Phys. Lett.* **2004**, *393*, 51–56.
(34) Vydrov, O. A.; Scuseria, G. E. *J. Chem. Phys.* **2006**, *125*, 234109.
(35) Chai, J. D.; Head-Gordon, M. *J. Chem. Phys.* **2008**, *128*, 084106.
(36) Song, J. W.; Hirosawa, T.; Tsuneda, T.; Hirao, K. *J. Chem. Phys.* **2007**, *126*, 154105.
(37) Grimme, S. *Wiley Interdisciplinary Rev.: Comput. Mol. Sci.* **2011**, *1*, 211–228.
(38) Grimme, S.; Antony, J.; Ehrlich, S.; Krieg, H. *J. Chem. Phys.* **2010**, *132*, 154104.
(39) Bera, P. P.; Schaefer, H. F., III. *Proc. Natl. Acad. Sci. U.S.A.* **2005**, *102*, 6698–6703.
(40) Garrec, J.; Patel, C.; Rothlisberger, U.; Dumont, E. submitted, **2011**.
(41) Loos, P.-F.; Dumont, E.; Laurent, A. D.; Assfeld, X. *Chem. Phys. Lett.* **2009**, *475*, 120–123.
(42) This intramolecular hydrogen bond tends to be reinforced as a continuum model for solvation is used. It can be proposed that this correction tends to increase the partial atomic charges on the atoms implicated in this stabilizing interaction. In turn, the approaching distance d is further increased.
(43) Vokacova, Z.; Budesinsky, M.; Rosenberg, I.; Schneider, B.; Sponer, J.; Sychrovsky, V. *J. Phys. Chem. B* **2009**, *113*, 1182–1191.
(44) Blumberger, J.; Lamoureux, G.; Klein, M. L. *J. Chem. Theor. Comput.* **2007**, *3*, 1837–1850.
(45) The deviation from the π-stacked mode constitutes a severe deficience as the offset will not a priori be constant along a series of

products and in turn blurs the theoretical prediction in terms of activation energies and endothermicities.

(46) Boese, A. D.; Martin, J. M. L. *J. Chem. Phys.* **2004**, *121*, 3405–3416.

(47) Ceron-Carrasco, J. P.; Zúñiga, J.; Requena, A.; Perpete, E. A.; Michaux, C.; Jacquemin, D. *Phys. Chem. Chem. Phys.* **2011**, *13*, 14584–14589.

(48) Hong, I. S.; Carter, K. N.; Sato, K.; Greenberg, M. M. *J. Am. Chem. Soc.* **2007**, *129*, 4089.

(49) Munzel, M.; Szeibert, C.; Glas, A. F.; Globisch, D.; Carell, T. *J. Am. Chem. Soc.* **2011**, *133*, 5186–5189.